Site-Directed Solid-State NMR Measurement of a Ligand-Induced Conformational Change in the Serine Bacterial Chemoreceptor†

Owen J. Murphy III,‡ Frank A. Kovacs,§ Erin L. Sicard,‡ and Lynmarie K. Thompson*,‡,§

Graduate Program in Molecular and Cellular Biology and Department of Chemistry, University of Massachusetts, Amherst, Massachusetts 01003-4510

Received June 30, 2000; Revised Manuscript Received October 30, 2000

ABSTRACT: The challenging nature of studies of membrane proteins has made it difficult to determine the molecular mechanism of transmembrane signaling. For the bacterial chemoreceptor family, there are crystal structures of the internal and external domains, structural models of the transmembrane domain, and evidence for subtle ligand-induced conformational changes, but the signaling mechanism remains controversial. We have used a novel site-directed solid-state NMR distance measurement approach, using $^{13}C^{19}F$ REDOR, to measure a ligand-induced change of 1.0 ± 0.3 Å in the distance between helices α1 and α4 of the ligand-binding domain in the *intact, membrane-bound* serine receptor. This distance change is shown not to be due to motion of the side chain and thus is due to motion of either the α1 or the α4 helix. Additional distance measurements can be used to determine the type of backbone motion and to follow it to the cytoplasm, to test and refine current proposals for the mechanism of transmembrane signaling. This is a promising general method for *high-resolution* measurements of local structure in intact, membrane-bound proteins.

The mechanisms of transmembrane signaling are poorly understood, in part because of the lack of structural information due to difficulties inherent in applying X-ray crystallography or solution-state NMR[1] for complete structure determination of membrane-bound receptors. The bacterial chemoreceptors of *E. coli* and *Salmonella* and the chemotaxis pathway they regulate have been extensively studied (*1*), providing an excellent system for probing the mechanism of signal transmission across the lipid bilayer. Furthermore, evidence suggests that the mechanism is likely to be general: it has been shown that aspartate binding regulates the intrinsic tyrosine kinase activity of a chimeric receptor consisting of the bacterial aspartate receptor ligand-binding and transmembrane domains fused with the insulin receptor intracellular domain (*2*). The 60 kDa chemotaxis receptors provide sensory input for a phosphorylation cascade controlling the swimming direction of the bacterium (*3*). A number of studies indicate that ligand binding induces conformational changes in the dimeric receptor, which are thought to transmit the signal (*4*−*15*). There is also evidence that the clustering of dimers may be involved in the signaling mechanism (*15*−*22*).

Structure determination of the periplasmic fragment of the aspartate receptor from *Salmonella* (Tar_s) reveals a dimer, where each subunit consists of a four-helix bundle labeled α1−α4 (Figure 1A,C), with a pseudo-intersubunit four-helix bundle consisting of the α1 and α4 helices of each subunit (*5*−*8*). Analysis of the aspartate receptor fragment crystal structures has yielded two different proposed mechanisms for ligand-induced change: an ∼4° pivot motion between monomer subunits (*8*), or a 1.6 Å piston motion of the C-terminal helix (α4) relative to the other helices within one subunit (*10*). These ligand-induced changes are thought to be propagated by the transmembrane helices across the membrane to control the phosphorylation of the associated histidine-kinase, CheA, in the cytoplasm. Discrimination between these and other possible mechanisms requires direct structural measurements on the intact receptor.

Solid-state NMR distance measurements provide a powerful high-resolution tool for mapping local structure and structural changes in proteins. Magic-angle spinning (MAS) is used in solid-state NMR to average orientation-dependent interactions and thus narrow broad lines to increase resolution and sensitivity in the spectrum. Dipolar couplings are also removed, but can be reintroduced with techniques such as REDOR and rotational resonance (*23*). We [and others (*24*)] are extending the power of these methods by combining them with site-directed mutagenesis to target the measurements to site(s) of interest. Here we report the application of this approach to measure selected distances in the ligand-bound and ligand-free signaling states of the serine chemoreceptor of *E. coli* (Tsr_{ec}). We have measured a ligand-induced conformational change in the tertiary structure of the *intact, membrane-bound* receptor using ^{13}C-observed, ^{19}F-dephased REDOR NMR ($^{13}C^{19}F$ REDOR).

† This research was supported by U.S. Public Health Service Grant GM47601, an award from Research Corporation, and a NSF Young Investigator Award (to L.K.T.).

* To whom correspondence should be addressed. Phone: 413-545-0827, FAX: 413-545-4490, E-mail: thompson@chem.umass.edu.

‡ Graduate Program in Molecular and Cellular Biology.

§ Department of Chemistry.

[1] Abbreviations: CPMAS, cross-polarization with magic-angle spinning; IPTG, isopropyl thio-β-D-galactoside; kDa, kilodalton; NMR, nuclear magnetic resonance; REDOR, rotational echo double resonance; rmsd, root-mean-square deviation; SDS−PAGE, sodium dodecyl sulfate−polyacrylamide gel electrophoresis; Tar_s, aspartate receptor of *Salmonella*; TM, transmembrane; Tsr_{ec}, serine receptor of *E. coli*.

10.1021/bi0015109 CCC: $20.00
Published on Web 01/10/2001

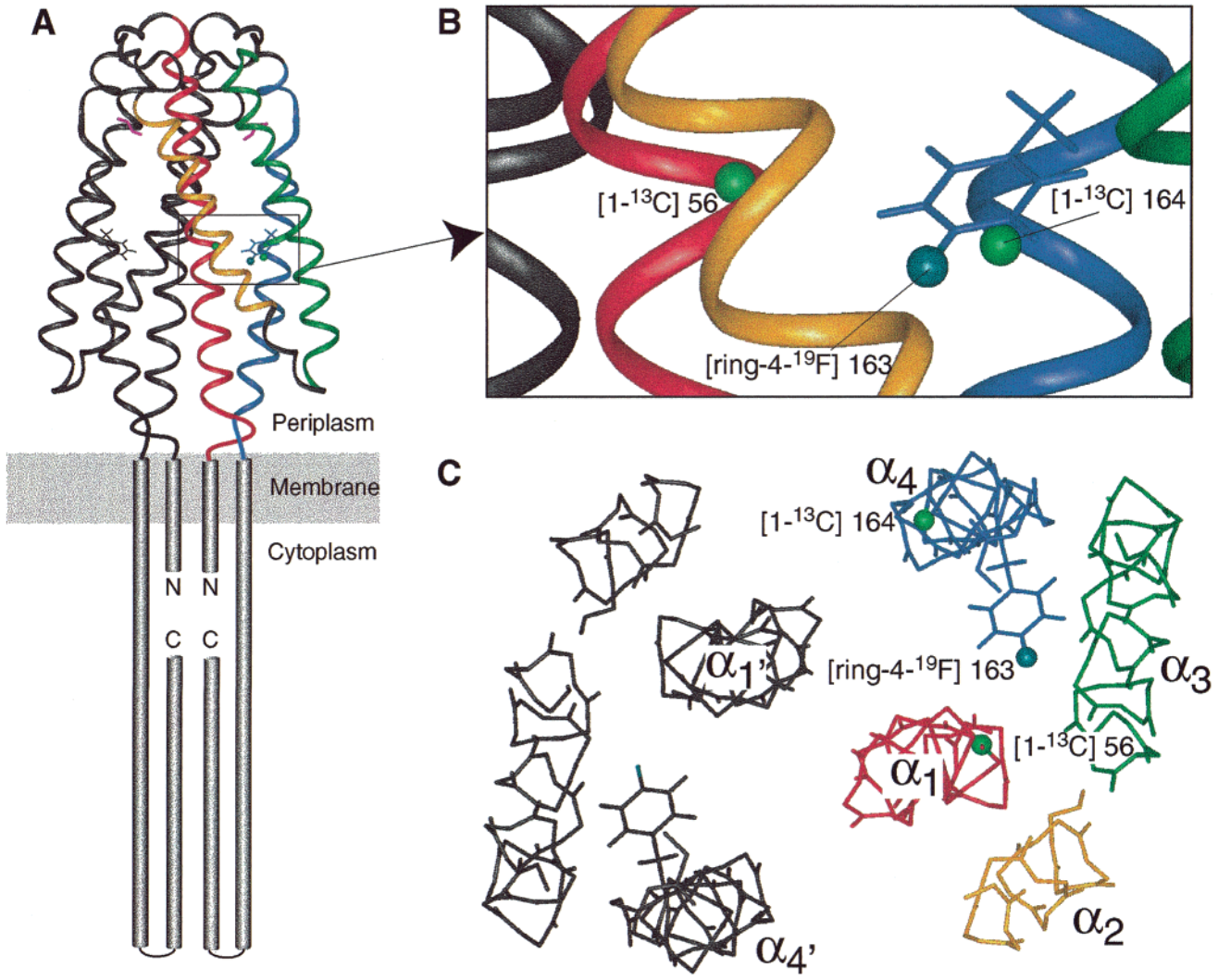

FIGURE 1: Structural model of the periplasmic domain of Tsr_{ec} depicting the label sites for the distances measured by REDOR NMR. (A) Side view backbone ribbon trace of the symmetric periplasmic fragment dimer of the aspartate receptor of *Salmonella* (2VLT in PDB) (*8*) adjoined as in (*49*) to helical transmembrane and cytoplasmic domains, pictorially represented with cylinders. The two bound ligands are shown in pink. The four-helix bundle arrangement of one subunit of the dimer is set apart by color, with the N-terminal long α1 helix in red, the α2 helix in yellow, the α3 helix in green, and the C-terminal long α4 helix in blue. To model the sites of interest in Tsr_{ec}, residue Leu161 (corresponding to residue Phe163 in Tsr_{ec}) is changed to a Phe, with its $\chi 1$ rotamer position set at 180°. (B) Enlargement of the boxed area in (A) showing the location of the nuclei used to monitor the interhelical and intrahelical distances in the ligand-bound and ligand-free states of Tsr_{ec}. The interhelical (α1 to α4) REDOR experiment monitors the distance between the α1 backbone carbonyl carbon of residue 56 (green ball) and the side-chain ring *p*-fluoro (aqua-green ball) of residue 163 (Tar_s residue 161). The intrahelical REDOR experiment monitors the distance between the α4 backbone carbonyl carbon of residue 164 (Tar_s residue 162) and the side-chain ring *p*-fluoro of residue 163. (C) View down the dimer axis of the periplasmic domain (view from the end distal to the membrane; the prime after the helix designation denotes the other subunit).

MATERIALS AND METHODS

Mutagenesis. The gene encoding wild-type serine receptor (Tsr_{ec}) was expressed from pHSe5 (*25*), with the *tsr* insert flanked by unique *Bam*HI and *Hin*dIII sites. The point mutation S56C was incorporated into the wild-type gene in pHSe5 using the Inverse Polymerase Chain Reaction (IPCR) method (*26*). The point mutant E164C was incorporated into the wild-type gene in pHSe5 using the QuikChange method (Stratagene). The resultant vectors were identified as pOM56C and pOM164C.

Swarm Assays. Chemotaxis swarm assays were performed using *E. coli* strain HCB429 (*27*) [relevant genotype: Δ*(tsr)-7021,* Δ*(tar-tap)5201,* Δ*(tar)100, zbd*::Tn5] transformed with either pHSe5.tsr, pOM56C, pOM164C, or pUC9. Soft agar swarm plates were prepared as described in (*28*), with or without 0.1 mM L-serine. Two milliliter LB starter cultures were inoculated and grown to $OD_{600} = 0.4$ at 37 °C. Two microliters of culture was then spotted onto soft agar swarm plates by gently puncturing the surface and injecting cells below the surface. Plates were allowed to sit for 16 h at room temperature. Swarm diameters were then measured at ~1 h intervals with initial measurement equal to time zero. Each time point was the mean of six equivalent swarm ring diameter measurements. Linear regression analysis of plots of the swarm diameters (± standard deviation) vs time determined the best-fit value of the swarm rate (slope of the line) and its standard deviation.

Protein Expression and Labeling. E. coli strain DL39C [relevant genotype: *cysE::Tn5, aspC13, fnr-25, ilv12, tyrB507*], a multiauxotrophic strain [Cys-, Phe-, Tyr-, Asp-, Leu-, Ile-, Val- (leaky)], provides the background for the biosynthetic labeling of engineered receptors with 99% L-[1-

^{13}C]cysteine (Cambridge Isotopes, Cambridge, MA) and L-[ring-4-^{19}F]phenylalanine (Sigma Chemical, St. Louis, MO). DL39C was constructed from DL39CM, a gift from David LeMaster, Wadsworth Center, Albany, NY. Due to the toxicity associated with *p*-^{19}F-Phe (*29*) as the sole source of phenylalanine, a media shift technique was used for double labeling of Tsr_{ec} receptors. DL39C cells transformed with pOM56C or pOM164C were grown at 30 °C, with constant aeration (250 rpm rotator shaking) in defined media (*25*) containing 0.8 mM L-phenylalanine and 20 mg/L L-[1-^{13}C]-cysteine to mid-log phase (OD_{600} = 0.9−1.0). Cells were spun down and washed 2 times in 0.25 volume of 0.9% NaCl, and then resuspended in defined media containing 20 mg/L labeled cysteine and 1.0 mM L-[ring-4-^{19}F]phenylalanine. After resuspension, IPTG was added to 0.5 mM final concentration to induce expression, and growth proceeded at 30 °C with constant aeration for 3 h.

Isolation of Whole-Membrane Vesicles Containing Overexpressed Receptor. Whole-membrane vesicles of mixed inner- and outer-membranes containing overexpressed Tsr_{ec} receptor were prepared as described (*30*) with minor modifications, from the null chemoreceptor *E. coli* strain HCB429. Whole-membrane vesicles were used for in vitro methylation assays because in our experience these preparations are leaky to ligand. Thus, the predominantly inside-out vesicles, with the cytoplasmic domain accessible for CheR binding and methylation, will be leaky enough to allow ligand to bind to its site inside the vesicles and increase the methylation rate. Expression at 30 °C from mid-log 1 L cultures was induced by the addition of IPTG. Cells were then harvested and resuspended in a 25 mL/L culture of low-salt buffer: 0.1 M Na_2HPO_4/NaH_2PO_4, pH 7.2, 10% glycerol, 5 mM 1,10-phenanthroline, 2 mM phenylmethylsulfonyl fluoride (PMSF), 5 mM EDTA, and 5 mM DTT. Cells were lysed by passage through a French Press 2 times at 1000−1500 psi, and unbroken cells were removed by a low-speed spin, 10000g, for 20 min at 4 °C. Purification proceeded as described in (*30*), absent final high-salt washes. From 1 L of starting culture, ∼40 mg of Tsr protein in whole-membranes is made.

Isolation of Inner-Membrane Vesicles Containing Overexpressed Receptor. Inner-membrane vesicles were prepared by a gentle osmotic lysis protocol (*31*), for ligand-binding assays and NMR samples. Each inner-membrane preparation was purified from 4 × 1 L cultures. Three of the 1 L cultures were grown with both ^{13}C and ^{19}F labeling, harvested, and then divided in half for two parallel purifications, one of which was purified in the presence of 2 mM serine. Thus, a matched pair of ligand-free and ligand-bound receptor samples was prepared from 3 of the starting 4 L of culture. The final 1 L of cells was grown with *p*-^{19}F-Phe and unlabeled Cys. The purified inner-membrane suspensions were dialyzed against 20 mM sodium phosphate buffer, pH 7.0. For the two S56C-Tsr_{ec} samples and the two E164C-Tsr_{ec} samples, 45−60 mg/1.5 L of Tsr is prepared by this method. Total protein concentration is determined by BCA assay and a 40% receptor purity estimate based on densitometer scan of Coomassie-stained SDS−PAGE gels of membrane samples. Duplicate inner-membrane preparations containing labeled receptors showed 90% *p*-^{19}F-Phe incorporation by amino acid analysis (MCB core facility, University of Massachusetts, Amherst, MA). We expect exclusive incorporation of the 99% L-[1-^{13}C]cysteine at position 56 or 164 in Tsr due to the cysteine auxotrophy of DL39C.

Ligand-Binding Assays. Ligand-binding assays were performed on detergent-solubilized membranes, thereby ensuring full access of all binding sites to serine ligand. A [^{3}H]serine displacement assay similar to the procedure described in (*32*) was used to measure ligand-binding affinities; 200 μL reactions contained ∼100 μL of receptor-containing membranes, 1 mM EDTA, 2 mM 1,10-phenanthroline, 25 mM Tris-HCl, pH 7.5, 1% *n*-octyl-β-D-glucoside, and varying amounts of [^{3}H]serine (1, 4, 10, 20, or 40 μM at a specific activity of 1 Ci/mmol). Reactions were incubated for 15 min and split into 2 × 95 μL volumes; to one was added excess cold serine (2 mM), to the other distilled water. After a 15 min incubation, soluble [^{3}H]serine was separated from receptors using Amicon MWCO-10 filter units by centrifuging the aliquots at 10000*g* for 10 min. Triplicate volumes of each flow-through were added to 5 mL of scintillation cocktail and counted to determine $[Ser]_{total}$ (aliquot chased with cold Ser) and $[Ser]_{free}$ (aliquot chased with water). $[Ser]_{bound} = [Ser]_{total} - [Ser]_{free}$ was plotted vs $[Ser]_{total}$ and fit to the 1:1 binding equation:

$$[Ser]_{bound} = \frac{1}{2}\left\{K_D + [S]_{total} + [R]_{total} - \sqrt{(K_D + [S]_{total} + [R]_{total})^2 - 4[S]_{total}[R]_{total}}\right\}$$

where $[R]_{total}$ is the concentration of receptor dimer, to obtain the equilibrium dissociation constant for Ser (K_D) for the stronger first binding event (the weaker binding of the second ligand to the receptor dimer was not measured).

Methylation Response Assays. In vitro methylation reactions of wild-type and point mutant chemoreceptors were performed as described (*19*), with slight modifications. The methyltransferase cheR (30 μM stock) was provided by Robert M. Weis, University of Massachusetts at Amherst. Individual reactions consisting of 20 μM receptor (in whole-membrane vesicles), 3 μM cheR, ± 2 mM L-serine, in 50 μL total volume of 50 mM Na_2HPO_4/NaH_2PO_4, pH 7.5, 3 mM DTT, 1 mM PMSF, were preincubated for 1 h at 4 °C. Reactions were started by the addition of 200 μM ^{3}H-SAM (0.1 Ci/mmol specific activity) at room temperature. Methylation incorporation was stopped by spotting a 10 μL aliquot onto 1 cm^2 Whatman filter paper and immediately immersing it in a 5% TCA bath for 2 × 10 min. Filter papers containing precipitated receptors were rinsed 2 × 5 min in 100% methanol and air-dried. Filter papers were placed in 5 mL of scintillation cocktail and counted. Each rate was computed from a single point, the methylation level at 5 min. Eight such measurements were made for each sample to obtain the mean and standard deviation. Under these conditions, the wild-type receptor rate (no Ser) was 0.046 ± 0.006 methyl group (Tsr subunit)$^{-1}$ min^{-1}.

NMR Sample Preparation. Inner-membrane vesicle suspensions containing overexpressed labeled mutant serine receptor were pelleted for 1 h at 100000*g* (45 000 rpm in a Beckman Ti70 rotor). The hydrated pellet is estimated to have a volume of 1 mL and have a Tsr_{ec} concentration of 0.8−1.0 mM. The pelleted membranes were kept at 4 °C and packed into a 5 mm silicon nitride rotor (Doty Scientific), or the pellet was quick-frozen in liquid N_2 and placed under vacuum and lyophilized for 12 h, after which the lyophilized

sample was packed into a 5 mm silicon nitride rotor. The packed 5 mm rotors contained approximately 400 nmol of lyophilized Tsr_{ec} or 200 nmol of frozen Tsr_{ec}. All lyophilized sample REDOR experiments were performed at 280 K, and the frozen sample experiments were performed at 241 K.

NMR. Cross-polarization with magic-angle spinning (CP-MAS) ^{13}C solid-state NMR spectra were acquired on an ASX300 spectrometer (Bruker Instruments) equipped with controllers to maintain constant temperature and MAS speeds. The tuning frequencies for the triple channel REDOR NMR experiment are 75.47 MHz (^{13}C), 300.13 MHz (^{1}H), and 282.4 MHz (^{19}F). Experiments were performed with MAS speeds of 5 kHz ± 3 Hz using a 5 mm supersonic triple resonance (HFX) probe (Doty Scientific). $^{13}C^{19}F$ REDOR measures dipolar couplings by collecting a pair of ^{13}C spectra: the full signal, S_o, and the dipolar-dephased signal, S. Dipolar effects are reintroduced in the dephased spectrum (S) by ^{19}F π pulses every half and full rotor period, which change the sign of the $^{13}C-^{19}F$ dipolar coupling and thus prevent the MAS from averaging the dipolar coupling (*33*, *34*). The $^{13}C^{19}F$ REDOR pulse sequence (*35*) begins with sensitivity enhancement of the ^{13}C signal via ramped cross-polarization (*36*), followed by a dipolar evolution period of rotor-synchronized ^{19}F π pulses, followed by the acquisition of the ^{13}C spectrum. A single refocusing π pulse is applied to the ^{13}C spins at the midpoint of the dipolar evolution period. Cross-polarization was performed with a 2.5 ms contact time, a proton field strength of $\gamma B_1/2\pi = 50$ kHz, and a 14% ramp on the carbon power. The proton decoupling field was increased to 78 kHz during the REDOR dipolar evolution mixing period and to 60 kHz during signal acquisition. On the ^{19}F channel, $\gamma B_1/2\pi = 67$ kHz for the 180° pulses. Spectra were collected using the XWIN-NMR 1.3 software package (Bruker Instruments) on a Silicon Graphics Indy computer and analyzed using Kaleidagraph software package 3.0.2 (Abelbeck Software) on an Apple Power Macintosh 7600/120 computer.

$^{13}C^{19}F$ REDOR experiments were calibrated using a self-diluted polycrystalline [^{19}F]polycarbonate standard, poly-(oxycarbonyloxy-1,4-phenylene-isopropylidine-1,4-phenylene-oxycarbonyloxy-1,4-phenylene-isopropylidine-(3-fluoro)-1,4-phenylene (kindly provided by L. McDowell and J. Schaefer, Washington University). The polymer provides a self-diluted $^{13}C^{19}F$ spin-pair (the 3-fluoro, which occurs on every fourth ring, and the neighboring resolved C4 ring carbon resonance at 136 ppm) with a strong dipolar coupling of 2100 Hz (2.4 Å) (L. McDowell and J. Schaefer, personal communication). For this strong dipolar coupling, full REDOR dephasing of the signal occurs before 8 rotor cycles. Thus, a "shifted" REDOR pulse sequence (*37*), with the dephasing π pulse moved from the center of the rotor period to 0.1 times the rotor period, was used to reduce the effective dipolar coupling. $\Delta S/S_o$ data for 8 and 16 rotor cycles of dephasing were analyzed with the REDOR expression for a mirror-symmetric pulse sequence (*37*) to yield a slightly long r_{CF} = 2.55 Å. Since REDOR measurements often slightly overestimate the distance, this result demonstrates our protocol gives accurate measurement of ^{13}C to ^{19}F distances.

$^{13}C^{19}F$ REDOR NMR Data Analysis. S_o and S values were obtained by integration of the carbonyl resonance (168−182 ppm). These data were corrected for the ^{13}C natural-abundance contribution to S_o empirically, via comparisons of CPMAS spectra of the ^{13}C-labeled and unlabeled samples: the unlabeled sample prepared under the same conditions and at the same time as its labeled counterparts indicates the natural-abundance contribution in the labeled samples. The CPMAS spectrum of the unlabeled sample was adjusted to match the intensities in the aromatic and CH_2/CH_3 regions of the labeled spectra, to correct for differences associated with the total amount of sample packed per rotor. Integrals of the scaled carbonyl peak regions were used to derive the fractional contribution of the label: $F = (I_L - I_U)/I_L$, where I_L = integral of the labeled carbonyl and I_U = integral of the unlabeled carbonyl. S_o data were corrected by multiplication by this factor, F. A further correction multiplied S_o by 0.9 to account for the fact that 90% of the ^{13}C sites had a neighboring *p*-^{19}F-Phe: $(\Delta S/S_o)_{corrected} = \Delta S/(S_o \times F \times 0.9)$. An additional natural-abundance correction to the ΔS value was needed in order to correct for the *p*-^{19}F-Phe dephasing of the natural-abundance carbonyl resonance, which must be subtracted ($\Delta S_{labeled} - \Delta S_{unlabeled} = \Delta S_{uniqueCys}$, after appropriate scaling). This was measured in REDOR experiments on the E164C unlabeled sample (which lacks the ^{13}C label but is labeled with *p*-^{19}F-Phe). This correction was significant for the intrahelical distance measurement, [1-^{13}C]Cys164 to [ring-4-^{19}F]Phe163: the correction increased the distance from 8.9 to 10.1 Å. For the shorter 5.8−6.8 Å interhelical distances, the E164C unlabeled sample spectra indicated that the correction would change the distances by an insignificant amount (0.1−0.2 Å), but would increase the error slightly from ±0.1 to ±0.2 Å.

The error due to spectral noise (which is likely to be the dominant error in such dilute spin samples) was estimated as follows. The error for a peak height measurement is the standard deviation of a noise region of the spectrum; for an integral measurement, this standard deviation is multiplied by the increment per point (set to 1 for all integrations) and the square root of the number of points integrated (because as signal adds in proportion to n, noise adds in proportion to the square root of n).

REDOR data, $(\Delta S/S_o)_{corrected}$, were fit to the following equation (*37*) to obtain the dipolar coupling, D_{CF} (Hz), and its standard deviation:

$$\frac{\Delta S}{S_o} = 1 - \frac{1}{4\pi}\int_{\beta=0}^{\pi}\int_{\alpha=0}^{2\pi} \cos[(D_{CF}N_cT_r)2\sqrt{2}\,\sin 2\beta\,\sin\alpha]\partial\alpha\,\sin\beta\,\partial\beta$$

where the dipolar evolution period = N_cT_r (number of rotor cycles × rotor period) and α and β are the azimuthal and polar angles, respectively, describing the orientation of the internuclear vector with respect to the sample rotation axis. The curve fitting was performed with pro Fit 5.1 (QuantumSoft) using the Levenberg−Marquardt nonlinear least-squares method. The distance r (meters) between the two spins is related to the dipolar coupling by:

$$D_{CF}\,(\text{Hz}) = (\mu_o/4\pi)\gamma_C\gamma_F h/4\pi^2(r^3)$$

where the magnetic constant $(\mu_o/4\pi)$ = permeability of a vacuum, $\gamma_C\gamma_F$ = the gyromagnetic ratios of ^{13}C and ^{19}F, and h = Planck's constant.

A REDOR curve describing two isolated spin-pairs equals the additive contribution of each spin-pair's REDOR curve

Table 1: Functional Assays on Engineered Receptors[a]

receptors	methylation rate response ratio	binding affinity [K_D (μM)]	chemotactic swarm rate (mm/h) (+)Ser	(−)Ser
wild-type Tsr_{ec}	1.5 ± 0.4	10 ± 4	1.9 ± 0.2	0.8 ± 0.3
S56C-Tsr_{ec}	1.6 ± 0.4	16 ± 6	1.9 ± 0.3	0.8 ± 0.3
E164C-Tsr_{ec}	1.7 ± 0.7	15 ± 6	1.8 ± 0.2	0.8 ± 0.1

[a] In vitro methylation rates are based on measured methylation levels of the receptor 5 min after addition of ^{3}H-SAM. The response ratio represents the methylation rate in the presence of 2 mM serine divided by the rate in the absence of serine. An in vitro radioactive displacement assay was used to measure the ligand affinity for each receptor. Chemotaxis swarm rates on (+)Ser- and (−)Ser-containing soft agar plates are reported.

as described in (*38*). For the asymmetric ligand-bound model, such an average curve was used to fit the $(\Delta S/S_o)_{corrected}$ data, with one spin-pair fixed at 5.8 Å, to obtain the best-fit distance for the other spin-pair.

RESULTS AND DISCUSSION

Mutagenesis for Selective Distance Measurements. Proposed mechanisms involving ligand-induced motions of the receptor helices can be tested by measuring distances between helices in the intact receptor. We chose $^{13}C^{19}F$ REDOR (*33*, *34*, *39*) for its ability to measure relatively long distances (up to 12 Å) between ^{13}C and ^{19}F nuclei in isolated spin-pairs. Fluorinated aromatic amino acids have been incorporated into a number of proteins without perturbing their function (*40*), and *p*-F-Phe labeling of the Asp receptor periplasmic domain has previously been shown not to perturb ligand binding (*9*). Site-directed mutagenesis was used to introduce unique cysteine residues (Tsr_{ec} contains no native cysteines) at target sites close to an isolated phenylalanine residue at position 163 on the α4 helix in the periplasmic domain of the intact receptor. The chosen sites were on helix α1 (Ser56 replaced by Cys) for measurement of an interhelical distance to probe for ligand-induced motions of α1 or α4, and on helix α4 (Glu164 replaced by Cys) for measurement of an intrahelical distance to define the Phe side-chain conformation (see Figure 1). The 2 engineered serine receptors, S56C-Tsr_{ec} and E164C-Tsr_{ec}, were labeled biosynthetically by incorporation of L-[1-^{13}C]cysteine at the unique Cys position and L-[ring-4-^{19}F]phenylalanine at the 13 Phe positions. For $^{13}C^{19}F$ REDOR experiments, only ^{19}F-spins within ~12 Å cause dipolar dephasing of a ^{13}C nucleus. Although the details of the structure of this domain may differ between Tsr_{ec} and Tar_s, the 39% sequence identity (in the helical regions) in this domain (*41*) suggests that the overall four-helix bundle architecture should be retained. Thus, the Tar_s crystal structure can be used to estimate the distances from the engineered Cys residues to the four phenylalanines in the periplasmic domain of Tsr_{ec}. The Phe at position 163 is predicted to occur within 12 Å of the [1-^{13}C]- at positions 56 or 164; the next nearest Phe residue is estimated to be ≈20 Å away from these sites. Thus, the engineered, labeled receptors contain isolated ^{13}C, ^{19}F spin-pairs for distance measurements that monitor local conformational change upon ligand binding to the receptor.

Three assays were used to evaluate the functionality of the engineered receptors (Table 1). In vivo swarm rates comparable to those of wild-type receptors indicate that the engineered receptors retain the ability to mediate chemotaxis on serine-containing soft agar plates. Inner- and whole-membrane vesicles containing overexpressed receptors were isolated for in vitro assays. Ligand-binding assays demonstrate that the engineered receptors have binding affinities within the reported 5−27 μM range for wild-type receptors (*42*, *43*). Finally, the expected ligand-induced increase in methylation rate was observed (*19*), indicating that the engineered receptors retain transmembrane signaling.

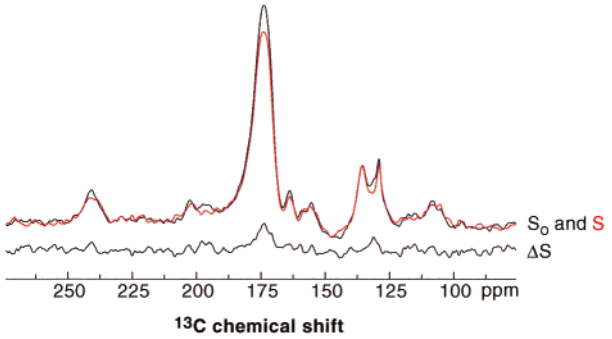

FIGURE 2: One set of REDOR spectra of the lyophilized S56C-Tsr_{ec} sample. A total of 37 000 transients were acquired for both the S_o and S spectra with a recycle delay of 1 s, spinning speed of 5 kHz, and 48 rotor cycles of dipolar evolution (9.6 ms). The dipolar dephasing of the carbonyl resonance (174 ppm) is the difference between the full-echo spectrum (S_o) in black and the dipolar dephased spectrum (S) in red. Spectral subtraction of S from S_o gives the difference spectrum (ΔS).

$^{13}C^{19}F$ REDOR NMR Distance Measurements. $^{13}C^{19}F$ REDOR was used to measure the interhelical distance from [1-^{13}C]Cys56 (α1) to [ring-4-^{19}F]Phe163 (α4). Figure 2 presents one set of S_o (full intensity), S (dipolar-dephased), and $\Delta S = S_o - S$ spectra of 1-^{13}C-Cys, *p*-^{19}F-Phe-labeled intact S56C receptors bound to inner-membrane vesicles. Integration of the carbonyl resonance (182−168 ppm) provided $\Delta S/S_o$ values that were corrected empirically for the 1% ^{13}C natural-abundance contribution to the S_o peak area (see Materials and Methods). $(\Delta S/S_o)_{corrected}$ data were plotted versus dipolar evolution time and fit to a REDOR curve to obtain the distance. The REDOR experiment probing the α1/α4 interface (Figure 3) indicates that the best-fit [1-^{13}C]Cys56 to [ring-4-^{19}F]Phe163 distance is 5.8 ± 0.2 Å in the ligand-free receptor state (open circles are best-fit by the solid line) and 6.8 ± 0.2 Å in the ligand-bound state (filled circles are best-fit by the dashed line). This analysis assumes ligand binding changes the interhelical distance equally in both subunits of the dimeric receptor. An alternate analysis (dotted line, see below), which assumes an asymmetric change restricted to one subunit, results in a larger (2.2 Å) change in the distance to 8 Å. Data obtained on lyophilized (Figure 3A) and frozen (Figure 3B) samples are compatible with the same distances. Thus, ligand binding induces a change of at least 1.0 ± 0.3 Å in the α1/α4 interhelical distance within a subunit.

A similar REDOR experiment (Figure 4) was used to determine the side-chain conformation of Phe163. For this long-distance measurement, a correction was needed for the REDOR dephasing of the natural-abundance carbonyls by the *p*-F-Phe residues. This was performed on a matched receptor sample labeled with *p*-F-Phe and no ^{13}C-Cys, as described under Materials and Methods. In the apo-state (open diamonds) and ligand-bound state (filled diamonds)

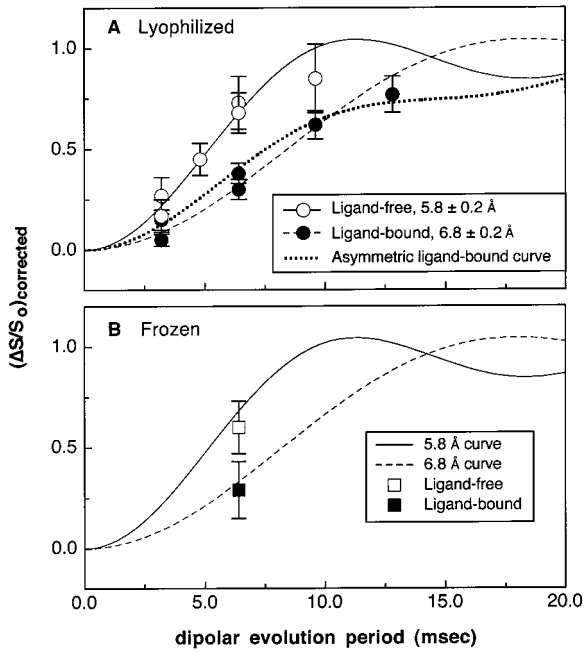

FIGURE 3: Interhelical distance measurements: S56C-Tsr$_{ec}$ ($\Delta S/S_o$)$_{corrected}$ REDOR data and best-fit REDOR curves. (A) Lyophilized [1-^{13}C]Cys56 (α1) to *p*-^{19}F-Phe163 (α4) distance measurements. Ligand-free S56C-Tsr$_{ec}$ data (open circles) for 16, 24, 32, and 48 rotor cycles of dephasing are best-fit (solid line) by a dipolar coupling of 147 ± 9 Hz, corresponding to a distance of 5.8 ± 0.1 Å. Ligand-bound S56C-Tsr$_{ec}$ data (filled circles) for 16, 32, 48, and 64 rotor cycles of dephasing are best-fit (dashed line) by a dipolar coupling of 90 ± 4 Hz, corresponding to 6.8 ± 0.1 Å. A natural-abundance correction would not change this distance significantly (see Materials and Methods), but would increase the error to ±0.2 Å. This analysis assumes that ligand binding causes both halves of the receptor dimer to move equally. An alternative asymmetric ligand-bound receptor model assumes half of the dimer does not move. For this case, the ligand-bound S56C-Tsr$_{ec}$ data are fit to an average REDOR dephasing curve describing two isolated spin-pairs (*38*), with one spin-pair held at a distance of 5.8 Å. The best-fit (dotted line) distance for the other spin-pair is 8.0 ± 0.5 Å (dipolar coupling of 56 ± 10 Hz). (B) Frozen [1-^{13}C]-Cys56 (α1) to *p*-^{19}F-Phe163 (α4) distance measurements. 32 rotor cycle experiments performed at 241 K on ligand-free (open square) and ligand-bound (filled square) frozen S56C-Tsr$_{ec}$ samples are consistent with the same distances as the lyophilized data. All experiments were performed at a MAS speed of 5000 Hz and a recycle delay of 1 s. The S_o and S spectra used to calculate ($\Delta S/S_o$)$_{corrected}$ are derived from 30 000−60 000 transients per spectrum for the lyophilized samples at 280 K, and from 120 000−172 000 transients for the frozen samples at 241 K.

of E164C-Tsr$_{ec}$, the [1-^{13}C]Cys164 to [ring-4-^{19}F]Phe163 distances are indistinguishable (best-fit distances of 10.2 ± 0.6 and 10.0 ± 0.5 Å, respectively). Thus, side-chain motion does not contribute to the ligand-induced 1 Å change in the interhelical α1/α4 distance. Using REDOR NMR, we have measured a ligand-induced conformational change of the helix backbone within the periplasmic domain of the intact membrane-bound serine chemoreceptor.

The dimeric nature of the receptor raises the question of whether the ligand-induced change in the α1/α4 interhelical distance occurs in one or both subunits. In the symmetric ligand-free receptor, the distance is 5.8 Å in both subunits. The preceding REDOR analysis, which assumes a single distance in the ligand-bound receptor as well, would mean both distances increase to 6.8 Å. The other simple extreme is that the ligand-induced change occurs in only one subunit

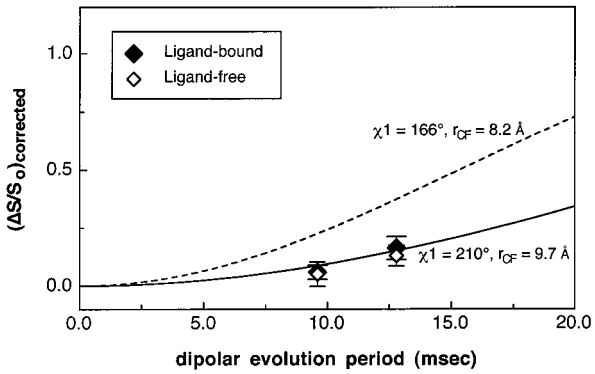

FIGURE 4: Intrahelical distance measurements: E164C-Tsr$_{ec}$ ($\Delta S/S_o$)$_{corrected}$ REDOR data and predicted REDOR curves for Phe163 rotamers near trans. Lyophilized [1-^{13}C]Cys164 (α4) to *p*-^{19}F-Phe163 (α4) distance measurements. Ligand-free E164C-Tsr$_{ec}$ data (open diamonds) for 48 and 64 rotor cycles of dephasing are best-fit by a dipolar coupling corresponding to 10.2 ± 0.6 Å. Ligand-bound E164C-Tsr$_{ec}$ data (filled diamonds) for 48 and 64 rotor cycles are best-fit (dashed black line) by a dipolar coupling corresponding to 10.0 ± 0.5 Å. Both data sets were corrected for ^{19}F dephasing of natural-abundance ^{13}CO (see Materials and Methods). Predicted distances and curves for two χ1 rotamers of the Phe ring which span the range of low-energy conformations (see Figure 5) in the crystal structure of the Tar$_s$ fragment.

and the other distance remains at 5.8 Å. For this asymmetric ligand-bound model, the REDOR data are fit to an average of REDOR curves for two different distances (Figure 3A, dotted line). This analysis yields an 8.0 ± 0.5 Å distance in the other subunit. Thus, the ligand-induced interhelical distance change is between 1.0 ± 0.3 Å (if both subunits change equally) and 2.2 ± 0.5 Å (if change is confined to a single subunit).

There are a number of caveats for REDOR measurements of absolute distances that do not compromise measurements of *relative* distances. Other protein impurities present in these heterogeneous membrane preparations could contain Cys (most likely without nearby *p*-F-Phe), which would reduce the fraction of the ^{13}C-Cys signal dephased in the experiment. Also, cumulative pulse imperfections and intrinsic high-frequency motions have been noted to compromise REDOR measurements of long distances (*44*). Receptor dynamics in the NMR samples could average the dipolar couplings. All of these effects would cause the REDOR-measured distances to be longer than the actual distances.

Comparison of the measured α1 to α4 distances of 5.8 and 6.8 Å in Tsr$_{ec}$ to the corresponding distances in the Tar$_s$ crystal structures is hampered by the fact that the Phe163 residue is not conserved. Thus, the first step in making this comparison is to determine the side-chain conformation of Phe163. The distance measurements presented in Figure 4 indicate χ1 is near a trans conformation in the Tsr$_{ec}$ structure. We also determined that such a side-chain conformation is compatible with the Tar$_s$ periplasmic fragment crystal structure, by replacing Leu161 (the corresponding residue in Tar$_s$) with Phe and finding the region of low energy conformations for this side chain using the Discover module in the Biosym InsightII software package. While fixing all other Tar$_s$ coordinate positions, the Phe ring was allowed to sample 360° of chi1 (χ1) and chi2 (χ2) space by 2° increments with the resulting overall energy calculated for each 180 × 180 matrix position. The contour plot of minimum energy (Figure 5) indicates that a conformation

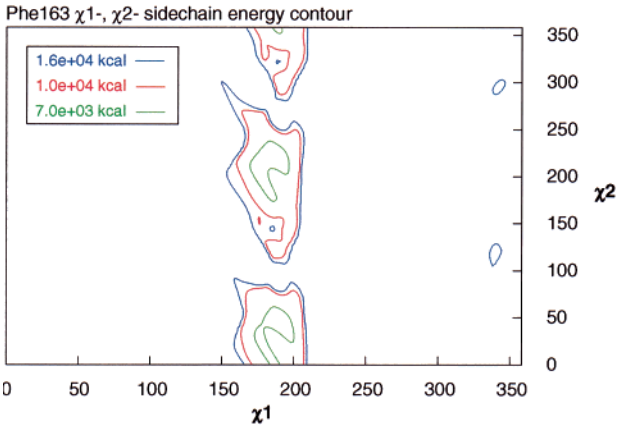

FIGURE 5: Contour plot of energy to determine what side-chain conformations of Phe are likely at the site of interest in the Tar_s structure. Atomic coordinates of the Tar_s fragment apo-structure (1LIH) (*7*) were used, with substitution of Phe for Leu at position 161 (virtually the same contours result when using the wild-type fragment apo-structure, 1VLS). All Tar_s coordinates are fixed except for the Phe side chain, which is allowed to rotate at 2° increments through 360° of $\chi1$ and $\chi2$ space as described in the text. Contour plot of the total receptor fragment energy (kcal) for each 2° increment of $\chi1$ and $\chi2$. The three low-energy contours plotted span a $\chi1$ range of ≈165−210°. An 8.5 Å cutoff for the Phe side chain was defined for the energy calculations, and repulsive van der Waals interactions dominated the changing energy terrain. The low-energy range includes the $\chi1$ value (≈180°) of the native residue Leu161 in the Tar_s (1LIH) fragment structure.

near trans ($\chi1 \sim 180°$) would be likely if the structure is similar to the Tar_s structure. Therefore, for the Phe substituted into the Tar_s structure, we assign $\chi1$ in this low energy range (≈165−210°) to check whether our interhelical distance measurement of 5.8 Å in Tsr_{ec} is consistent with that predicted in the Tar_s structure. With $\chi1 = 196°$, the corresponding interhelical distance in the Tar_s fragment structure is 5.8 Å (ligand-free structure 1LIH). This provides further evidence for a conserved tertiary structure within the chemotaxis receptor family, previously suggested by primary sequence comparison (*41*, *45*−*47*) and by $^{15}N^{13}C$ REDOR measurements in the ligand-binding pocket of Tsr_{ec} (*35*).

Despite the consistency between the distance measured in the ligand-free receptor and that predicted by the corresponding crystal structure, the measured 1 Å ligand-induced *change* in the interhelical distance is larger than that predicted by the Tar_s crystal structures. Again with $\chi1 = 196°$, the corresponding interhelical distance in the Tar_s fragment structure is 6.0 Å in the ligand-bound structure 2LIG, a change of only 0.2 Å. This difference is likely to be due to differences between the samples studied by NMR and crystallography. This NMR study was performed on lyophilized membranes containing *intact* Tsr_{ec}; the X-ray studies were performed on crystalline *fragments* of Tar_s.

The validity of using lyophilized samples in this case is established by REDOR NMR experiments conducted on frozen membranes: the frozen and lyophilized data fall on the same REDOR curve fit for the lyophilized data, indicating the lyophilized protein has the same absolute distances. Furthermore, the same ligand-induced change in interhelical distance was measured on two separate lyophilized sample pairs. The consistency of the REDOR results for lyophilized and frozen samples also suggests that dynamics, which would likely differ in the two sample types, are not affecting the distance measurement. Thus, the differences between the ligand-induced changes observed by NMR and crystallography are likely to be due to differences between the two receptor types or between the intact receptor and receptor fragments.

Site-Directed Solid-State NMR Provides High-Resolution Distances on Intact Receptors. The importance of measuring the ligand-induced structural change in the *intact* receptor is demonstrated by the fact that different ligand-induced changes are observed in crystal structures of different Tar_s fragments. Thus, the ligand-induced changes observed in the periplasmic *fragments* may not fully reflect changes in the native receptor. Different ligand-induced structural changes are observed in two different crystal structure pairs (1LIH, 2LIG and 1VLS, 2VLT in the protein database). In the disulfide-cross-linked (Cys36−Cys36′) fragment pair (1LIH, 2LIG), an intrasubunit 1.6 Å piston motion is observed (*10*). By following the same protocol for superimposing the structures, we observe the piston in the cross-linked structure pair, but we do not observe the piston in the wild-type, uncross-linked structure pair [1VLS, 2VLT, which was unavailable at the time of the analysis leading to the piston model (*10*)]. The intersubunit 3−4° pivot motion has been observed in both crystal structure pairs (*8*), but the pivot axis is shifted by over 15 Å (from the ligand binding site area in the wild-type proteins to the cross-link area in the cross-linked proteins). Clearly, these subtle conformational changes are easily perturbed in the fragment crystals. It is likely that neither fragment structure pair fully mimics the native receptor. The disulfide cross-link helps to retain the native association of the truncated helices (α1 and α4, which extend through the transmembrane region as TM1 and TM2 in the native receptor) but may also reduce intersubunit motions. Therefore, the real mechanism could be some combination of both pivot and piston motions with the possibility of larger distance changes than those seen by analysis of either crystal structure pair. Thus, it is important to augment the high-resolution picture of the receptor domains provided by crystallography (*5*−*8*, *48*, *49*) with selected high-resolution measurements of ligand-induced distance changes in the intact receptor system, to map the actual conformational change.

Our REDOR results also complement a recently published EPR study of the intact aspartate receptor which found evidence for ligand-induced changes of ∼1 Å in four interhelical distances across the α1-TM1/α4-TM2 interface (*4*). These results were interpreted to support a ∼1 Å piston motion of the α4-TM2 helix. The NMR approach presented here provides the means for obtaining the *high-resolution* distance constraints needed to more precisely map the pattern of changes characteristic of such a piston motion. The high sensitivity of the EPR method has enabled the measurement of a number of distances in both receptors and receptor complexes with CheA and CheW, which is critical since some aspects of receptor structure and behavior may differ when uncomplexed. The EPR study yielded the important result that the distance changes appear to be similar with and without CheA and CheW (*4*).

It is important to note that the geometry of the interhelical distance measurement is critical to the interpretation of any observed distance changes. This is illustrated in the simple cartoon model presented in Figure 6, in which interhelical

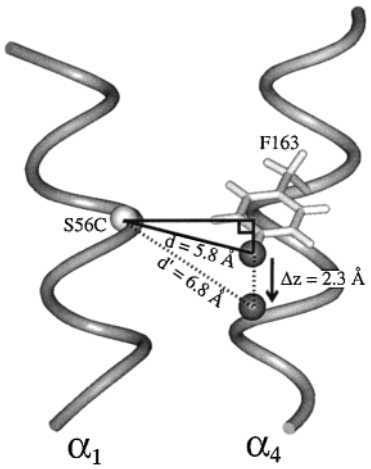

FIGURE 6: Cartoon model of a pure piston motion of the α4 helix—one of many possible motions compatible with the measured distance change. Tar_s coordinates for portions of the α1 and α4 helices were used to make the drawing. The *z* axis is defined as the long axis of the protein (roughly parallel to the helix axes), and the interhelical distances measured by NMR are represented by $d = 5.8$ Å and $d' = 6.8$ Å. To obtain the geometric constraint needed to interpret the data (the angle θ between the interhelical distance vector and the helix axes), the Phe163 $\chi 1$ was set to 196°, which makes $\theta = 75°$ and $z = 1.6$ Å (the vertical distance for the ligand-free state represented by the black triangle). The ligand-induced increase to $d' = 6.8$ Å, represented by the dashed lines, then corresponds to $\Delta z = 2.3$ Å. See text for discussion of other possibilities.

distances are represented by *d* and distances along the long axis of the receptor axis (roughly parallel to the helix axes) are represented by *z*. The significance of the measured ligand-induced $\Delta d = 1$ Å depends critically on the angle between the interhelical distance vector and the *z* axis, which is unknown. We can make an initial estimate of this geometry using the Tar_s crystal structure with a Phe side chain substituted at the position corresponding to Phe163 and $\chi 1 = 196°$, which is most compatible with our distance measurements. These assumptions result in $z = 1.6$ Å in the structure (black triangle in Figure 6 for the ligand-free state), and the ligand-induced $\Delta d = 1$ Å from 5.8 to 6.8 Å corresponds to a $\Delta z = 2.3$ Å. Thus, one simple conformational change consistent with our measurements is a 2.3 Å pure piston motion of the α4 helix. However, the magnitude of the piston motion depends on the assumed geometry: with the above assumptions which place the 5.8 Å distance vector 74° from the *z* axis, a $\Delta d = 1$ Å (measured) would correspond to a $\Delta z = 2.3$ Å. With a different geometry, placing the 5.8 Å distance vector 45° from the *z* axis, a $\Delta d = 1$ Å (measured) would correspond to a $\Delta z = 1.3$ Å piston. This demonstrates that interhelical vectors perpendicular to the axis of motion are relatively insensitive to small piston motions, and that using interhelical distance change measurements to measure piston motions of helices requires knowledge of the geometry. Thus, additional high-resolution distance measurements are critical in order to determine the geometry and to distinguish different types of motions of the helices at this site.

In summary, we report the first high-resolution measurement of a ligand-induced distance change in an intact, membrane-bound receptor. The measured 1 Å change in the distance between the α1 and α4 helices proves that the native serine receptor undergoes a ligand-induced intrasubunit conformational change, and is potentially consistent with the proposal that ligand binding induces a 1.6 Å piston motion of the α4 helix (*10*). Additional site-directed solid-state NMR measurements in progress should provide a detailed picture of the local structure in both signaling states of the intact, membrane-bound serine receptor. Measurements at other sites can be used to test for intersubunit pivot motions (with intersubunit distance measurements) and for propagation of any observed motions to the other receptor domains. These experiments will yield insight into the ligand-induced conformational change and the mechanism of transmembrane signaling in bacterial chemoreceptors.

The use of mutagenesis to direct solid-state NMR distance measurements provides a powerful general method for making high-resolution distance measurements at sites of interest for probing structure and mechanism. This will be a valuable approach for advancing our understanding of other important membrane protein systems.

ACKNOWLEDGMENT

We thank F. Dahlquist (University of Oregon) for the pHSe5.tsr plasmid, L. C. Dickinson, G. Entzminger (Doty Scientific), and A. Bielecki (Bruker Instruments) for assistance with the NMR instrument and probes, E. Voigtman for advice on error analysis, and R. Weis and L. Gierasch for helpful discussions.

REFERENCES

1. Falke, J. J., Bass, R. B., Butler, S. L., Chervitz, S. A., and Danielson, M. A. (1997) *Annu. Rev. Cell Dev. Biol. 13*, 457−512.
2. Biemann, H. P., Harmer, S. L., and Koshland, D. E., Jr. (1996) *J. Biol. Chem. 271*, 27927−27930.
3. Bourret, R. B., Borkovich, K. A., and Simon, M. I. (1991) *Annu. Rev. Biochem. 60*, 401−441.
4. Ottemann, K. M., Xiao, W., Shin, Y. K., and Koshland, D. E., Jr. (1999) *Science 285*, 1751−1754.
5. Milburn, M. V., Prive, G. G., Milligan, D. L., Scott, W. G., Yeh, J., Jancarik, J., Koshland, D. E., Jr., and Kim, S. H. (1991) *Science 254*, 1342−1347.
6. Yeh, J. I., Biemann, H. P., Pandit, J., Koshland, D. E., and Kim, S. H. (1993) *J. Biol. Chem. 268*, 9787−9792.
7. Scott, W. G., Milligan, D. L., Milburn, M. V., Prive, G. G., Yeh, J., Koshland, D. E., Jr., and Kim, S. H. (1993) *J. Mol. Biol. 232*, 555−573.
8. Yeh, J. I., Biemann, H. P., Privé, G. G., Pandit, J., Koshland, D. E., Jr., and Kim, S. H. (1996) *J. Mol. Biol. 262*, 186−201.
9. Danielson, M. A., Biemann, H. P., Koshland, D. E., Jr., and Falke, J. J. (1994) *Biochemistry 33*, 6100−6109.
10. Chervitz, S. A., and Falke, J. J. (1996) *Proc. Natl. Acad. Sci. U.S.A. 93*, 2545−2550.
11. Chervitz, S. A., and Falke, J. J. (1995) *J. Biol. Chem. 270*, 24043−24053.
12. Hughson, A., and Hazelbauer, G. (1996) *Proc. Natl. Acad. Sci. U.S.A. 93*, 11546−11551.
13. Tatsuno, I., Homma, M., Oosawa, K., and Kawagishi, I. (1996) *Science 274*, 423−425.
14. Gardina, P. J., and Manson, M. D. (1996) *Science 274*, 425−426.
15. Cochran, A. G., and Kim, P. S. (1996) *Science 271*, 1113−1116.
16. Maddock, J. R., and Shapiro, L. (1993) *Science 259*, 1717−1723.
17. Li, G., and Weis, R. M. (2000) *Cell 100*, 357−365.
18. Liu, Y., Levit, M., Lurz, R., Surette, M. G., and Stock, J. B. (1997) *EMBO J. 16*, 7231−7240.
19. Li, J., Li, G., and Weis, R. M. (1997) *Biochemistry 36*, 11851−11857.

20. Weerasuriya, S., Schneider, B. M., and Manson, M. D. (1998) *J. Bacteriol. 180*, 914−920.
21. Bray, D., Levin, M. D., and Morton-Firth, C. J. (1998) *Nature 393*, 85−88.
22. Long, D. G., and Weis, R. M. (1992) *Biochemistry 31*, 9904−9911.
23. Garbow, J. R., and Gullion, T. (1995) in *Carbon-13 NMR Spectroscopy of Biological Systems* (Beckmann, N., Ed.) pp 65−115, Academic Press, Inc., San Diego.
24. Studelska, D. R., Klug, C. A., Beusen, D. D., McDowell, L. M., and Schaefer, J. (1996) *J. Am. Chem. Soc. 118*, 5476−5477.
25. Muchmore, D. C., McIntosh, L. P., Russell, C. B., Anderson, D. E., and Dahlquist, F. W. (1989) *Methods Enzymol. 177*, 44−73.
26. Hemsley, A., Arnheim, N., Toney, M. D., Cortopassi, G., and Galas, D. J. (1989) *Nucleic Acids Res. 17*, 6545−6551.
27. Wolfe, A. J., Conley, M. P., Kramer, T. J., and Berg, H. C. (1987) *J. Bacteriol. 169*, 1878−1885.
28. Weis, R. M., and Koshland, D. E., Jr. (1988) *Proc. Natl. Acad. Sci. U.S.A. 85*, 83−87.
29. Richmond, M. H. (1962) *Bacteriol. Rev. 26*, 398−420.
30. Chervitz, S. A., Lin, C. M., and Falke, J. J. (1995) *Biochemistry 34*, 9722−9733.
31. Gegner, J. A., Graham, D. R., Roth, A. F., and Dahlquist, F. W. (1992) *Cell 70*, 975−982.
32. Biemann, H. P., and Koshland, D. E., Jr. (1994) *Biochemistry 33*, 629−634.
33. Gullion, T., and Schaefer, J. (1989) *J. Magn. Reson. 81*, 196−200.
34. Gullion, T., and Schaefer, J. (1989) in *Advances in Magnetic Resonance* (Warren, W. S., Ed.) pp 57−83, Academic Press, New York.
35. Wang, J., Balazs, Y. S., and Thompson, L. K. (1997) *Biochemistry 36*, 1699−1703.
36. Metz, G., Wu, X., and Smith, S. O. (1994) *J. Magn. Reson. A 110*, 219−227.
37. Hing, A. W., and Schaefer, J. (1993) *Biochemistry 32*, 7593−7604.
38. Goetz, J. M., and Schaefer, J. (1997) *J. Magn. Reson. 127*, 147−154.
39. McDowell, L. M., Lee, M., McKay, R. A., Anderson, K. S., and Schaefer, J. (1996) *Biochemistry 35*, 3328−3334.
40. Danielson, M. A., and Falke, J. J. (1996) *Annu. Rev. Biophys. Biomol. Struct. 25*, 163−195.
41. Jeffery, C. J., and Koshland, D. E., Jr. (1993) *Protein Sci. 2*, 559−566.
42. Clarke, S., and Koshland, D. E., Jr. (1979) *J. Biol. Chem. 254*, 9695−9702.
43. Lin, L. N., Li, J., Brandts, J. F., and Weis, R. M. (1994) *Biochemistry 33*, 6564−6570.
44. Pan, Y., Gullion, T., and Schaefer, J. (1990) *J. Magn. Reson. 90*, 330−340.
45. Boyd, A., Kendall, K., and Simon, M. I. (1983) *Nature 301*, 623−626.
46. Russo, A. F., and Koshland, D. E., Jr. (1983) *Science 220*, 1016−1020.
47. Le Moual, H., and Koshland, D. E., Jr. (1996) *J. Mol. Biol. 261*, 568−585.
48. Bowie, J. U., Pakula, A. A., and Simon, M. I. (1995) *Acta Crystallog., Sect. D 51*, 145−154.
49. Kim, K. K., Yokota, H., and Kim, S. H. (1999) *Nature 400*, 787−792.

BI0015109